Chapter 8
Wireless Powered Sensor Networks

Wanchun Liu, Salman Durrani, and Xiangyun Zhou

8.1 Wireless Sensor Networks

The first wireless sensor network (WSN) was originally invented by the United States Military in the 1950s to detect and track Soviet submarines [1]. The network, which consisted of acoustic sensors, was distributed in the Atlantic and Pacific oceans. In the 1980s, the United States Defense Advanced Research Projects Agency (DARPA) started the distributed sensor network program which boosted the civilian and scientific research on WSNs. Thanks to the advances in semiconductor, networking and material science technologies in the past a few decades, the ubiquitous deployment of large-scale WSNs has finally come true. The state-of-the-art WSNs have many applications such as micro-climates measurement on farms, habitat monitoring, volcano monitoring, structural monitoring, vehicle tracking, human presence detection in homes and offices, electrical/gas/water metering.

For instance, consider the applications of WSNs in Australia as an example [2]. In South Australia, WSNs have been widely used to monitor the growing of grapes. Sensors measure the temperature, light, wind speed, humidity, and soil moisture and provide information for analysis, in order to optimize plant growth and prevent crop loss. In Victoria, a wireless sensor network of 100 nodes was deployed over

This work was supported by the Australian Research Council's Discovery Project Funding Scheme (Project number DP140101133).

W. Liu (✉) • X. Zhou
Research School of Engineering, The Australian National University,
Canberra 2601, ACT, Australia
e-mail: wanchun.liu@anu.edu.au; xiangyun.zhou@anu.edu.au

S. Durrani
College of Engineering and Computer Science, The Australian National University,
Canberra, Aust Capital Terr, Australia
e-mail: salman.durrani@anu.edu.au

D.N.K. Jayakody et al. (eds.), *Wireless Information and Power Transfer: A New Paradigm for Green Communications*, DOI 10.1007/978-3-319-56669-6_8

a 1 km square region of forest in the Dandenong Ranges. The network monitors in real-time, a range of environmental parameters to improve situational awareness, such as the event of bush fires. In Melbourne, in order to solve the noise pollution problem, a WSN has been deployed across the central business district to measure sound level. A noise map of the city is generated by the data collected from the sensors, which is then used to manage noisy areas. In Sydney, WSNs are deployed to detect and indicate where open parking is located in the city streets to reduce traffic congestion.

The future Internet-of-Things (IoT), which is going to connect tens of billions of low-complexity wireless devices such as sensors and wearable computing devices, can be treated as a advanced evolution of WSN. The IoT will enable new applications such as smart cities, home automation, and e-healthcare. One of the most important implementation challenge of the IoT is that the finite battery capacity sensor nodes have a limited lifetime and thus require regular battery replacements [3]. This kind of battery replacement for massive number of IoT nodes is difficult or even infeasible as many sensors are deployed in hazardous environments or hidden in walls, furniture, and even in human bodies.

One immediate solution is to use large batteries for longer lifetimes, however, the increased size, weight, and cost may not be affordable for the massive number of sensors. Another solution is to adopt low power hardware, but at the cost of lesser computation ability and lower transmission ranges. To effectively address the finite node lifetime problem, an alternative technique, i.e., energy harvesting powered WSN is the most promising solution.

8.2 Energy Harvesting Wireless Sensor Networks

Generally speaking, energy harvesting (EH) means harvesting energy from the ambient environment such as solar, wind and thermal energy, or other energy sources such as foot strike, finger strokes, and body heat, and converting it to electrical power/energy. In theory, a sensor node can be powered perpetually as long as the harvested energy source is continuously available. Figure 8.1 illustrates the basic architecture of an EH WSN, which consists of multiple sensors and one sink. The sensors are able to harvests energy from a solar panel and may also harvests energy from other energy sources such as RF signals emitted by power beacons or base stations (which will be discussed in the next subsection).

More precisely, an EH sensor consists of six modules which are illustrated in Fig. 8.2: a micro-controller (not included in the figure for brevity), EH module, battery, sensing modulo, transmitter(and receiver), and data buffer. The sensor first needs to convert the ambient energy arrival into a direct current (DC) signal by the EH module, which is then used to charge the battery of the sensor. Powered by the harvested energy, the sensing module senses its relevant parameters and saves the sensed data into the data buffer, and the transmitter transmits the sensed data to the sink.

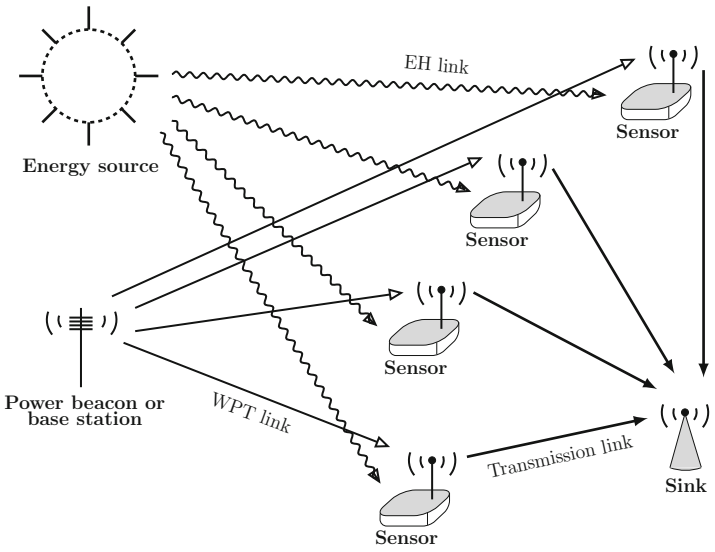

Fig. 8.1 Illustration of EH WSN

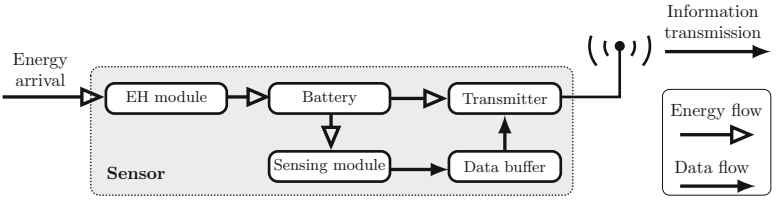

Fig. 8.2 Illustration of the components of a wireless sensor node

Table 8.1 Environmental energy harvesting power (reproduced from [5])

Source	Average harvested energy
Solar panel	15 mW/cm^2
Light (indoor)	10–100 μW/cm^2
Airflow	0.4–1 mW/cm^3
Vibrations	200–380 μW/cm^3
Thermoelectric	40–60 μW/cm^2
Piezoelectric	100–330 μW/cm^3

The EH rate of different energy sources are listed in Table 8.1. It is straightforward to see that EH from a solar panel can provide the highest EH rate. In addition, solar energy is the most easily accessible energy source and there are lots of existing WSN applications based on it. For example, the outdoor multi-target tracking networks [4], such as the zebra tracking and the turtle habitat monitoring networks in the USA.

8.2.1 WSN Power Consumptions

There are three main energy costs in wireless sensors, which are summarized in [5] as

1. Energy cost of RF transmission and reception. This is the energy consumption of the RF components of the transmitter (and also the receiver), such as the mixer and the analog to digital converter (ADC).
2. Energy cost of information sensing and processing. This is the energy consumption of the sensor chip and the ADC of the sensing module.
3. Energy cost of other basic processing while being active. This is the energy consumption of the micro-controller of the wireless sensor node. The processing unit, which is generally associated with a small storage unit, performs tasks, processes data, and controls the functionality of other components in the sensor node.

The power consumptions for processing, sensing, and transmission/reception for most commonly used WSN nodes are summarized in Tables 8.2, 8.3, and 8.4, respectively. In Table 8.2, we list two micro-controllers PXA271 and ATmega 128/L, which are used in WSN nodes Inote2 and MicaZ, respectively. We also include three micro-controllers of TI's low voltage low power series. Comparing TI's MSP430F2132 with ATmel's ATmega 128/L, we see that the active power consumption is significantly reduced. In Table 8.3, we list six sensor chips with the functions of dual-axis accelerometer, three-axis accelerometer, pressure sensing, light sensing, temperature sensing, and thermopile sensing. We see that the power consumption of different types of sensors varies greatly. In Table 8.4, we list six commonly used 2.4 GHz Low Power Transceiver for the IEEE 802.15.4 standard. Comparing TI's CC2502 with Freescale's MC1321, it is easy to see that MC1321's power consumption is almost doubled compared to CC2502 in the receive mode, while the transmit power consumption is almost the same.

We see that the energy cost of processing and sensing is much smaller compared to the energy cost of transmission, and this is the reason why majority of the current work on EH WSNs has considered only the energy cost of transmission, while ignoring the energy cost of processing and sensing [6, 7].

However, the IoT will require various more complicated sensing functions, such as charge coupled device (CCD) or complementary metal oxide semiconductor (CMOS) image sensors that adopt array sensing, and high-rate and high-resolution acoustic and seismic sensors [8] (and the references therein). The energy cost of sensing in this scenario can actually be higher than the energy cost of transmission. Moreover, as an emerging low power communication technique, backscatter communication [9], which does not have any active RF components and relies on passive RF signal reflection, has an ultra low power consumption roughly within a μW level when active for transmissions [10, 11]. Therefore, in these application scenarios, power consumptions for sensing are comparable to or even much higher

Table 8.2 Processor consumption

Features	PXA271	ATmega 128/L	TMS320c5535	MSP430BT5190	MSP430F2132
Manufacturer	CPU	MCU	DSP	MCU	MCU
Company	Intel	Atmel	TI	TI	TI
Voltage supply	3 V	5 V	1.05 V	3 V	2.2 V
CPU frequency	13 MHz	12 MHz	50 MHz	20 MHz	1 M
Active mode power	44.2 mW	125 mW	7.5 mW	9 mW (RAM program execution)	0.55 mW
Standby mode power	1.72 mW (idle 8.5 mW)	8.5 mW	0.26 mW	3.6 μW	1.54 μW
Wake up time	<0.6 ms	<1.5 ms	> 30.5 μs	<5 μs	<1 μs
Start time (from power down)	<136.65 ms	>4.12 ms	>8 ms	<0.15 ms	<2 ms
Notions	Used by Imote2 (High-performance wireless sensor network node)	Used by commercial off-the-shelf sensor plat form such as, MicaZ, Mica2	TI low voltage low power series	TI low voltage low power series	TI low voltage low power series

Table 8.3 Sensor consumption

Features	ADXL202JE	ADXL345	MS5534AM	TSL2550D	PGA309-ht	LMP91051
Manufacturer	Analog devices	Analog devices	Intersema	TAOS	TI	TI
Function	Dual-axis accelerometer	Three-axis accelerometer	Barometric pressure sensor	Ambient light sensor	Temperature and pressure sense	Thermopile sensor
Voltage supply	3.5 V	2.5 V	3 V	3.3 V	3 V	3.3 V
Active mode power	1.75 mW	58 μW	3 mW	1 mW	3.6 mW	11.88 mW
Standby mode power	< 0.084 mW	0.25 μW	0.01 mW	< 0.03 mW	0	0.247 mW
Data conversion time	2 ms	> 0.3 ms	< 35 ms	400 ms	< 0.2 ms	<10 μs
Begin to sleep	–	1.4 ms	–	–	0	2 μs
Wake up time	–	1.4 ms	–	1 s	0	1 ms

Table 8.4 Transceiver consumption (reproduced from [5])

Features	CC2520	CC2430	CC2590	JN5139	MC1321	EM1250
Manufacturer	TI	TI	TI	Jennic	Freescale	Ember
Radio frequency (GHz)	2.4	2.4	2.4	2.4	2.4	2.4
Bit rate (kbps)	250	250	250	250	250	250
Supply voltage (V)	1.8–3.8	2.0–3.6	2.2–3.6	2.2–3.7	2.0–3.4	2.1–3.6
Sleep current (μA)	1	0.5	0.1	0.2	1	1
Rx current (mA)	18.5	27	3.4	34	37	29
Tx current min (mA)	16.2(−18 dBm)	–	–	–	20.9(−28 dBm)	19(−32 dBm)
Tx current max (mA)	33.6 (5 dBm)	27 (0 dBm)	22.1 (12 dBm)	35 (3 dBm)	30 (0 dBm)	33 (5 dBm)

than that of transmission/reception. The first study is [12] that considers a WSN energy allocation problem taken into account both the sensing and transmission power consumptions.

8.2.2 EH Models

In order to evaluate the performance of EH-based communications, we need to model the EH process first. Most of the studies have modeled EH processes as a time-discrete process or a block-by-block process, due to the fact that sensors, in practice, operate in a time-block-based manner, i.e., transmission and sensing tasks are processed in one or several time blocks. In other words, we care about how much energy is harvested in different EH time blocks, rather than the entire time-continuous energy harvesting process within each of the block. In general, the harvested energy in each EH block could either remain constant or change from block to block. These EH fluctuations in time-domain are characterized by the coherent time. The coherence time is the time interval (i.e., the number of EH time blocks) within which the harvested energy does not change much.

There are three EH models listed below, as illustrated in Fig. 8.3.

1. Deterministic EH Model. Deterministic energy arrival is the most simple EH model. It is a proper model when the coherence time of the EH process is much larger than the duration of the entire communication session, such as EH by solar panel on clear days. Since the deterministic EH model is very simple, it is commonly adopted to evaluate the performance of EH-based WSN communications [13–15].
2. Non-Causal EH Model. Non-causal EH model is an ideal EH model that the future EH process is entirely known at the beginning of transmission. If the non-causal EH information is known at a node, it can adopt the optimal energy scheduling strategy and achieves the maximum communication performance. Therefore, non-causal EH model is useful to provide a performance upper bound.
3. Random EH Models. The most popular EH model in the recent years is the random EH model in which the EH process is regarded as random processes. In general, random EH process can be treated as a casual EH model. They are divided into two categories:

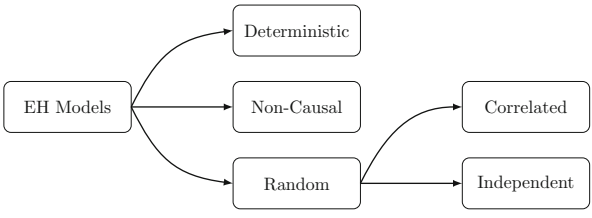

Fig. 8.3 Classification of EH models

a. Correlated EH process is an EH process that the harvested energy in the current time block, which is a random variable, is related to the harvested energy in the previous time blocks, i.e., a Markov EH model [6, 7, 16]. For example, in [17, 18], the EH process is modeled as an ON–OFF two-state a first-order discrete-time Markov process, where the harvested energy during an ON block is constant while there is no energy harvested in OFF blocks.
b. Independent EH process is an EH process that the harvested energy in the current time block is independent to the harvested energy in the previous time blocks, i.e., an i.i.d. EH model. For the i.i.d. energy arrival model, the available harvested energy in each time block follows i.i.d. continuous distribution [19–21]. In [21, 22], Bernoulli i.i.d. discrete EH process is considered.

8.2.3 Design and Performance Analysis

Most of the EH WSN design problems can be treated as energy/power scheduling/management problems under dynamic EH processes. If the allocated power usage in one time block is very high, an energy outage may happen in the next few time blocks in which the EH rate is very low and cannot support the relevant power consumptions, and thus causes performance losses. While if the allocated power usage is very low in one time block, an energy overflow may happen in the next a few time blocks in which the EH rate is very high and a finite battery cannot store all the available energy, and thus causes a waste of energy. Therefore, it is very important to carefully design the power scheduling protocols.

The power scheduling problem has basically two scenarios: offline and online, corresponding to non-causal and causal EH processes, respectively. The design targets of the power scheduling problems are mostly focused on average transmission throughput maximization during a certain time duration and transmission completion time minimization, and average delay minimization, such as [23–25], respectively. The required constraints of the optimization problems include the energy causality, i.e., not using energy in the future, and the battery capacity.

For the offline optimization problems, where the full knowledge of both the energy state information and the transmission channel state information are known before the beginning of transmission, when both the object function is a concave and the constraints are convex, the optimal power scheduling strategy can be found by solving Karush–Kuhn–Tucker conditions [23]. However, most of the EH power scheduling problems are not convex, and in this case, optimal (deterministic) dynamic programming policy and greedy policy are helpful [26]. The approach in the optimal dynamic programming policy is to break an optimization problem into sub-problems and then recursively find the optimal solutions to the sub-problems. The greedy policy also first breaks down the problem into sub-problems, but then it simply picks optimal choices for each sub-problem as the solution. However, such locally optimal (i.e., greedy) choices may result in a bad global solution. On the

other hand, the greedy policy has a much lower computation and space complexity compared to the optimal dynamic programming policy and usually provides an acceptable sub-optimal solution in some scenarios.

For the online optimization problems, the optimization only accounts for partial or full statistical knowledge of the EH and transmission channel fading dynamic processes, and the problem is usually solved as an online optimal power control problem. The most commonly used method is the stochastic dynamic programming [26, 27]. Formally, the stochastic dynamic policy has the same components as the deterministic one. The only difference is that for the stochastic dynamic programming, when evaluating each sub-problem, the long-term effect caused by the adopted strategy should be taken into account.

8.3 Wireless Power Transfer and Wireless Sensor Networks

Leveraging the far-field radiative properties of electromagnetic waves, wireless receivers are able to harvest energy remotely from RF signals radiated by RF signal emitters. This simple invention has been known long (a century ago) before the recent excitement about WPT. WPT techniques are considered popular because of the following two properties:

1. Wireless, which enables conveniently powering large-scale ubiquitous nodes without battery replacements or specific conventional EH sources, particularly for implanted in-body sensors. In other words, WPT technologies have the potential to make people's life truly wire free.
2. RF signals carry both energy and information at the same time, which enables wireless power and information transfer at the same time.

Compared to conventional EH techniques, WPT has another two advantages:

1. WPT is more controllable and does not rely on environmental EH sources.
2. RF EH devices, i.e., rectifier-based simple passive components, are suitable for large-scale WSNs and IoT nodes. This is in contrast to: solar-energy-based node is equipped with heavy solar panel, vibration-energy-based node is equipped with relatively complex mechanical construction, thermal-energy-based node is equipped with relatively large area thermoelectric generators, wind-energy-based node is equipped with big size wind turbine.

A summary of some of the industry studies about the available harvested RF power is listed in Table 8.5. Compared with the EH rate provided by the conventional ambient EH methods shown in Table 8.1, we see that the EH rate of the WPT techniques in general is much lower and decays rapidly with the distance with the RF signal emitter. This is the main problem of WPT. However, for low power WSNs, WPT is viable and an attractive solution.

Table 8.5 Wireless power transfer experimental data [28]

Source	Source power	Distance	Amount of energy harvested (μW)
Isotropic RF transmitter	4 W	15 m	5.5
Isotropic RF transmitter	1.78 W	25 m	2.3
Isotropic RF transmitter	1.78 W	27 m	2
TX91501 powercaster transmitter	3 W	5 m	189
TX91501 powercaster transmitter	3 W	11 m	1
Tokyo TV tower	48 kW	6.3 km	0.1–0.25
KING-TV tower (Seattle)	960 kW	4.1 km	60
KING-TV tower (Seattle)	960 kW	10.4 km	≥15.8

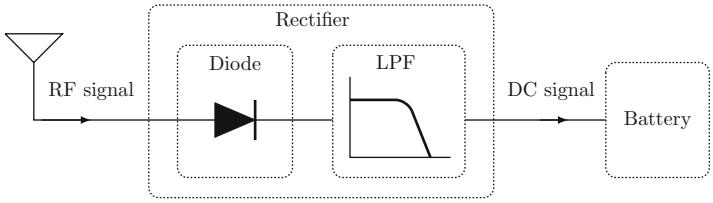

Fig. 8.4 Illustration of an RF-EH device

The architecture of a WPT-based wireless sensor is almost the same with an EH wireless sensor, as illustrated in Fig. 8.2. The only difference is that the EH module is replaced with an RF-DC converter, which is further discussed below.

8.3.1 RF-DC Converter

As mentioned above, an RF-EH device converting an RF signal to DC signal via a rectifier architecture is quite simple. It consists of a Schottky diode and a low pass filter (LPF), as illustrated in Fig. 8.4. To accurately measure how much available RF power captured by the antenna can be harvested, a proper model is required for the non-linear power conversion property introduced by the Schottky diode.

The I-V curve of a Schottky diode is illustrated in Fig. 8.5a, and it shows that only the positive part of the receive signal that is beyond a certain threshold can be harvested. The harvested power increases monotonically from zero when the receive signal power increases and is larger than the threshold. More precisely, the non-truncated part of the non-linear model can be written as

$$I = I_s \left(e^{\gamma V} - 1 \right), \tag{8.1}$$

where I_s is the saturation current, V is the voltage drop across the diode, and γ is the reciprocal of the thermal voltage.

Although the model (8.1) is precise, it is not tractable for general analysis. In [29], the authors take a Taylor expansion of the exponential function in (8.1), and

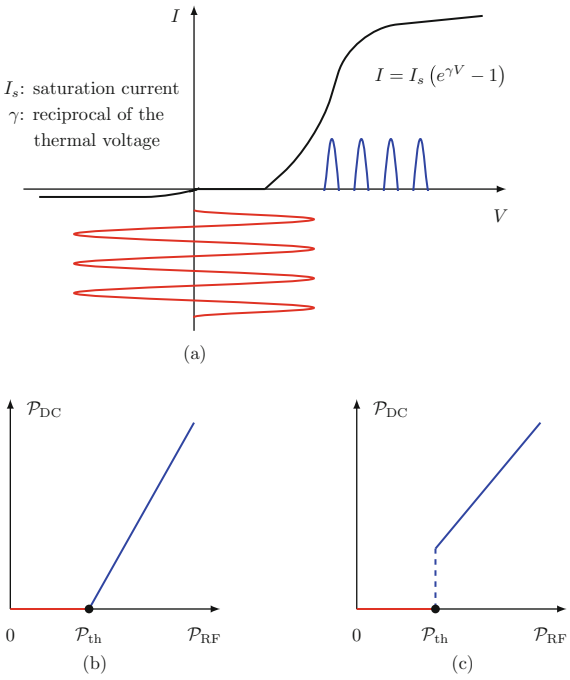

Fig. 8.5 Illustration of the models for RF-DC converter. (**a**) Accurate non-linear behavior of the Schottky diode. (**b**) Near-practical approximation. (**c**) Ideal approximation

the optimal waveform design is considered based on the simplified model. In [30], in order to better capture the truncated property of the Schottky diode, a non-linear model is considered as

$$\mathscr{P}_{\mathrm{DC}} = \frac{M}{1 + \exp\left(-a\left(\mathscr{P}_{\mathrm{RF}} - b\right)\right)}, \tag{8.2}$$

where M, a, b are the constant diode parameters, and $\mathscr{P}_{\mathrm{RF}}$ and $\mathscr{P}_{\mathrm{DC}}$ are the input RF power and the output DC power, respectively. Then an optimal resource allocation problem is considered for a multi-user simultaneous wireless information and power transfer system based on the non-linear model.

There are another two commonly considered simplified models for RF-DC power conversion, as illustrated in Fig. 8.5a,b.

1. For the near-practical model (Fig. 8.5b), the converted DC power is assumed to increase linearly with the received RF power only if it passes a threshold [31, 32].
2. For the ideal model (Fig. 8.5c), the converted DC power is assumed to be proportional to the RF power only if it is beyond the threshold [33, 34].

8.3.2 Network Model for WPT

There are three network models for WPT.

1. WPT only network, where energy transfer is in the downlink. In [35], the authors proposed a power beacon-based hybrid cellular network. In the network, mobile users are wirelessly powered by randomly deployed power beacons, which enables mobile users to have a much longer lifetime without battery replacement.

   Different scenarios such as single-/multi-user, relays, multi-carrier have been considered with WPT [29, 33, 36–41].

   In [33], wirelessly power transfer from a multi-antenna PB to single/multiple energy receivers is studied, where the optimal WPT strategy are obtained. In [36], a system consisting of a single power beacon and multiple energy receivers was considered, where the energy receiver can only do one-bit feedback. The optimal channel learning algorithm was also proposed for such a WPT system. In [37], the distributed WPT system with limited-feedback was studied, where a distributed channel learning method was proposed. In [38], WPT-based sensor networks were considered, where a large-scale sensor network is powered by randomly deployed power beacons. The sensor-active probability was also studied.

   In [39], the multiple power beacon placement problem was considered. The location of the power beacons was optimized which maximized the WPT powered communication network. In [40] and [41], WPT-based single- and bi-directional relay networks were considered, respectively, where the relay is wirelessly powered by the transmitter for relaying the information to the destination. The maximal throughput of such a relay networks was derived.

   In [29], WPT with multi-carrier waveform was considered, where waveform optimization method was proposed.
2. Simultaneous wireless information and power transfer (SWIPT) network, where energy and information are transferred simultaneously in the downlink by leveraging the property that RF signal carries both information and energy. In [33], the authors first proposed a practical SWIPT system, where the receiver can obtain information and energy simultaneously from the received signal by using a time-switching or power-splitting method, as illustrated in Fig. 8.6.

   For the time-switching-based SWIPT receiver, the RF antenna periodically switches between an information receiver and an energy receiver for information detection and energy harvesting, respectively. In this way, the SWIPT receiver is able to detect information for a certain percentage of time, and harvest energy in the rest of the time. For the power-splitting-based SWIPT receiver, the received RF signal is first split into two streams by a passive power splitter, and then one signal is sent to the information receiver and the other signal is sent to the energy receiver.

   SWIPT for a multi(MISO) broadcast channel was investigated in [42]. SWIPT in OFDM-based systems were further investigated in [43, 44]. Such systems are important, since 4G systems are based on OFDM. In [43], downlink

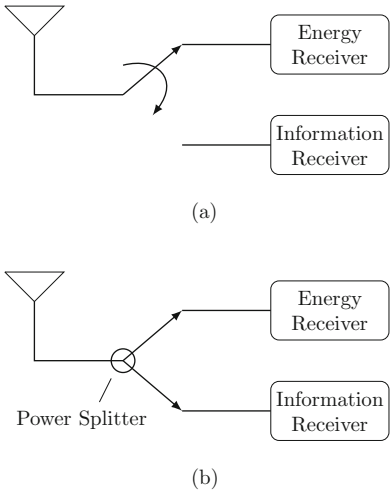

Fig. 8.6 SWIPT receivers. (**a**) Time-switching receiver. (**b**) Power-splitting receiver

OFDM-SWIPT in a multi-user system was studied, where the optimal resource allocation problem was solved. In [44], the resource allocation problem of an OFDM cellular system, which performs downlink SWIPT and uplink information transmission, was comprehensively studied.

3. Wireless powered communication network (WPCN), where energy is transferred in the downlink and information is transferred in the uplink. In [45], the authors first proposed the WPCN network model. In this network, mobile users harvest RF energy emitted by a base station, and transmit information to the base station when it has harvested enough energy. The WPCN is particularly useful in wireless sensor networks, since wireless sensors usually have very low downlink data rate but high uplink data rate, e.g., updating the sensed information to the sink.

8.3.3 WPT-Based WSN Transmission Protocols

Unlike traditional battery-operated communications, the available harvested RF power to the wirelessly powered nodes is time-variant due to the WPT channel fading. To smooth out the WPT channel randomness effect, the harvested RF energy is stored in an energy buffer, i.e., a battery or a super-capacitor, and there are two kinds of WSN transmission protocols that rely on the stored battery energy:

1. Harvest-use protocol, where the harvested energy in one time block is assumed to be used entirely within the same block. The harvest-use protocol can be adopted by WSNs with small battery storage [19, 33, 34, 45, 46], where the harvested energy should be used immediately, otherwise, the battery energy overflow occurs and leads to communication performance losses. On the other hand, the

performance analysis of harvest-use protocol-based WSNs is often tractable, which is hence adopted by many research studies. Therefore, the performance of a harvest-use protocol-based WSN can be treated as a lower bound of that obtained by an optimal transmission protocol.

2. Harvest-store-use protocol, where the harvested energy in one time block can be stored for future use. Since the harvested energy does not need to be consumed entirely, the harvest-store-use protocol provides a better transmission performance compared with the harvest-use protocol. The harvest-store-use protocol is adopted by WSNs with large battery storage [47–49]. In this case, the sensors do not need to use all the available energy at each time block, and thus can better utilize the available harvested energy and schedule its power consumption to improve the communication performance. In theory, in order to achieve a globally optimal performance of transmission, a sensor can adaptively change the transmit power in each time block depending on the current energy storage and the length of data queue. However, most of the WPT-based WSNs are simple devices, which require low-complexity protocols that do not allow adaptively changing the transmit power. Therefore, the widely adopted harvest-store-use protocol is a threshold-based protocol, which transmits with a constant power within a time block as long as there is sufficient energy for the transmission [47–49].

8.3.4 Performance Analysis

There is one important metric for each of the WPT network, SWIPT network, and WPCN, as shown below.

WPT efficiency is considered in WPT only networks, which is defined as

$$\eta_{\text{WPT}} = \frac{\mathscr{P}_{tx}}{\mathscr{P}_{rx}}, \tag{8.3}$$

where $\mathscr{P}_{tx}$ and $\mathscr{P}_{rx}$ are the transmit signal power and the harvested signal power at the transmitter and the receiver, respectively. WPT efficiently indicates the quality of a WPT protocol design, such as channel training-based energy transfer [50, 51], and multi-antenna energy beamforming [36, 37, 52].

Rate-energy region is considered in SWIPT networks, which is the boundary of all the achievable tradeoff for maximal information rate versus energy transfer [33, 34]. A large rate-energy region means the SWIPT network is more capable for simultaneously harvesting RF energy and detecting information, or the performance losses on information detection due to the RF energy harvesting is smaller.

Uplink throughput is the key metric for a WPCN. WPCNs encounter a doubly near-far problem due to the fact that a far sensor from the sink, which receives less wireless energy than a nearer sensor in the downlink, has to transmit with more power in the uplink to achieve the same reliable information transmission

rate [45]. Therefore, in order to achieve a better uplink throughput of a WSN, we need to properly design the downlink WPT and the uplink information transmission protocols. A time-division-multiple-access-based uplink–downlink user scheduling is proposed in [45].

8.4 Design Challenges

8.4.1 Sensor Power Consumption

Besides modeling the EH process, to accurately analyze the EH powered sensor behavior, we need an accurate model for sensor's energy costs. As discussed in the previous section, there are three main energy costs for a wireless sensors, and particularly, the energy costs of sensing and transmission/reception dominate the overall energy consumption.

Therefore, for a status monitoring WSN, we need to taken into account both the energy costs of sensing and transmission when analyze the performance of status monitoring.

8.4.2 The Age of Information

The recent internet-of-things brings ubiquitous wireless sensors together, which monitor environmental data and update them to the users. In this status monitoring application, we need the sensors to update their monitored status as timely as possible. The conventional metric to measure the timeliness of a WSN is update cycle, which measures the time elapsed from one status update at the sink to the next [48]. Update cycle captures how frequently the status information is updated at the user. For example, if the average update cycle of a WSN is 10 s, then we can expect that the status updates successfully at the user every 10 s. However, from the 10 s update cycle, we cannot see when the status was originally generated. For example, when a successful status is received/updated at the user, the status could be collected 9 s ago, which is not a fresh status, or 1 s ago, which is a fresh status. Measuring the freshness of the updated status has long been desirable, but it is only recently that it have been seriously considered and modeled in [53–55], and named as update age.

Since both the update frequency and freshness are related to determine how timely a status monitoring WSN is, we need both the update cycle and update age to accurately measure the timeliness of the status monitoring WSN. It was first proposed in a recent study [48] that using update cycle together with update age brings a comprehensive measure of the timeliness of a status monitoring WSN. The idea is simple that since update age and update cycle are complementary to each

other, i.e., update cycle does not reflect the update freshness at the sink whereas update age does not reflect the update frequency, the best way to evaluate the performance of a status monitoring WSN is to jointly utilize both of them.

8.5 WPT-WSN: Delay Analysis Considering Energy Costs of Sensing and Transmission

8.5.1 System Model

We consider a status monitoring scenario where a wirelessly powered sensor periodically transmits its sensed status information to a sink, as illustrated in Fig. 8.1. The sensor is able to harvest RF energy from a nearby power beacon. To complete the status monitoring task, the sensor has two main functions, i.e., sensing and transmission, each having individual energy cost. Before performing either sensing or transmission, the sensor first needs to spend a certain amount of time on EH. The harvested energy is stored in a half-duplex battery, which cannot charge and discharge at the same time [19]. Because the commercial battery capacity typically ranges from joules to thousands of joules [4], and the available harvested energy per second is only a few millijoules, as shown in Table 8.5, we assume that the battery has a sufficient capacity such that the amount of energy stored in the battery never reaches its maximum capacity.

We adopt a block-wise operation following the state-of-the-art EH sensor design practice [56]. Specifically, we assume that one sensing operation or one transmission is performed in one time block of duration T seconds, and sensing and transmission cannot occur within a same time block. In general, a sensor may spend different amounts of time on one sensing operation and one packet transmission [8]. Thus, in future study, the assumed protocol and analysis can be generalized to different sensing and transmission time durations. At the beginning of each block, the sensor makes a decision to perform either energy harvesting, sensing, or transmission depending on the current battery energy storage. Before the discussion of such sensing and transmission protocol, firstly, we need the following definitions of three types of time blocks:

1. Energy harvesting block (EHB): The sensor harvests RF energy and stores the energy in its battery. We consider that the wireless channel between the power beacon and the sensor suffers from independent and identically distributed (i.i.d.) block Rayleigh fading. In general, Rayleigh fading channel is commonly considered in the scenario where there is no line-of-sight, and there are sufficient scatters between the transmitter and the receiver. Note that if there is line-of-sight between the power beacon and the sensor, Rician or Nakagami fading channel model should be adopted, which is further studied in [48].

With the i.i.d. Rayleigh fading channel assumption for the WPT link, the harvested energy in each EHB follows the same exponential distribution and changes independently from block to block. Thus, we refer to the energy arrival process as exponential energy arrival process. The average EH rate is ρ Joules per block.

2. Sensing Block (SB): The sensor samples the environmental status information, and then processes and packs the sensed information into a data packet. The energy cost in a SB is denoted by $\mathscr{E}_{\mathrm{SB}}$ Joules.
3. Transmission Block (TB): The sensor transmits the data packet, which was generated from the last sensing operation, to the sink with energy cost $\mathscr{E}_{\mathrm{TB}}$ Joules, i.e., the transmit power is $\mathscr{P}_{\mathrm{TB}} = \mathscr{E}_{\mathrm{TB}}/T$. To indicate successful packet reception, the sink sends a one-bit feedback signal to the sensor after each TB. Note that the time and energy consumed for receiving the feedback signal at the sensor is negligible as compared to its packet transmission time. If the transmission is successful, we have a successful transmission block (STB); otherwise, we have a failed transmission block (FTB).

   The transmission outage, i.e., the probability of a TB being a FTB, is denoted by P_{out}. We assume that a transmission outage from the sensor to the sink occurs when the SNR at the sink γ is lower than SNR threshold $\gamma_0 = 40\,\mathrm{dB}$ [57]. The outage probability is

$$P_{\mathrm{out}} = \Pr\{\gamma < \gamma_0\}. \tag{8.4}$$

   The SNR at the sink is defined as [58]

$$\gamma = \frac{|h|^2 \mathscr{P}_{\mathrm{tx}}}{\Gamma d^{\lambda} \sigma^2}, \tag{8.5}$$

   where h is the sensor-sink transmission channel fading gain, Γ is a path loss factor which is assumed to be one [31] for simplicity, σ^2 is the noise power at the sink, d is the distance between the sensor and the sink, and λ is the path loss exponent.

   Also we assume that h is block-wise Rayleigh fading. Using (8.5), the transmission outage probability can be written as

$$P_{\mathrm{out}} = 1 - \exp\left(-\frac{d^{\lambda}\sigma^2\gamma_0}{\mathscr{P}_{\mathrm{tx}}}\right). \tag{8.6}$$

8.5.2 Sensing and Transmission Protocol

The time-varying EH process results in randomness in the delay for performing sensing and transmission. To properly design a sensing and transmission protocol for a status monitoring WSN, two issues need to be considered.

The first issue is about when to perform sensing. Considering the energy cost of sensing, it is necessary to harvest sufficient energy, $\mathscr{E}_{\mathrm{SB}}$, before a sensing operation. However, it is not a good choice to perform sensing as soon as the harvested energy reaches $\mathscr{E}_{\mathrm{SB}}$. Because there may not be sufficient energy left for transmission after the sensing operation, a certain amount of time for EH is required to prepare for transmission which results in unnecessary delay and makes the sensed status less timely. Therefore, to avoid such delays and make the update timely, we define the condition for the sensing operation to be when the harvested energy in the battery exceeds $\mathscr{E}_{\mathrm{SB}} + \mathscr{E}_{\mathrm{TB}}$. In this way, a transmission of sensed status information occurs immediately after the sensing operation (i.e., a SB is always followed by a TB).

The second issue is about whether we need a retransmission when a failed transmission (i.e., a FTB) occurs. Considering the energy cost of sensing, it is necessary to perform retransmission(s) if the first TB after a SB is failed, rather than drop the packet and perform the next sensing operation. However, an arbitrary number of retransmissions that make a status-information-containing packet to be eventually received by the sink should be prevented. This is because a very long retransmission process would make the updated status very untimely at the sink. Therefore, we impose a time window for retransmissions to control the delay caused by retransmissions. We denote W as the maximum number of time blocks after a SB, within which transmission and retransmission(s) of the currently sensed information can take place. Specifically, the *time window for retransmissions* is $W - 1$ time blocks, due to the fact that the first transmission always happens immediately after the SB.

We present the sensing and transmission protocol as follows, and the flowchart of the protocol is illustrated in Fig. 8.7.

(a) First, several EHBs are required to harvest enough energy, $\mathscr{E}_{\mathrm{SB}} + \mathscr{E}_{\mathrm{TB}}$, and then a SB and a TB occur immediately.
(b) If the TB is a STB, i.e., the transmission in the TB is successful, in order to prepare for the next sensing period, the sensor attempts to harvest energy, which may take several EHBs, until the battery energy exceeds $\mathscr{E}_{\mathrm{SB}} + \mathscr{E}_{\mathrm{TB}}$ again.
(c) If the TB is a FTB, i.e., the transmission in the TB fails, in order to prepare for a retransmission, the sensor has to go back to harvesting energy, which may take several EHBs, until the battery energy exceeds $\mathscr{E}_{\mathrm{TB}}$.
(d) Retransmission may occur several times until either one of the two conditions is met: (1) The sensed information is successfully transmitted to the sink, i.e., a STB finally occurs, or (2) the time window for retransmissions $W-1$ is reached but no STB occurs. Then, the data packet at the sensor is dropped, no matter successful retransmission or not, and the sensor goes back to harvesting energy for a new sensing operation.

An illustration of the sensing and transmission protocol with $W = 6$ is shown in Fig. 8.8. From the example, we see that two EHB occur first, after which the battery energy exceeds $\mathscr{E}_{\mathrm{SB}} + \mathscr{E}_{\mathrm{TB}}$, and then a SB together with a TB occurs. Although the TB is a FTB, after two retransmissions, a STB occurs. Then, after three EH

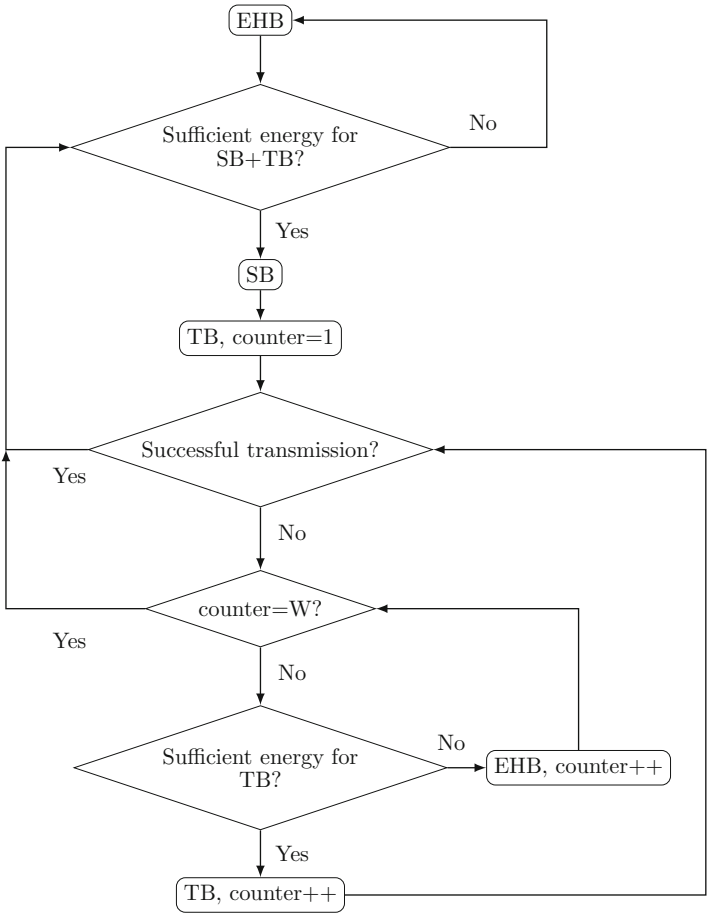

Fig. 8.7 Flowchart of the protocol

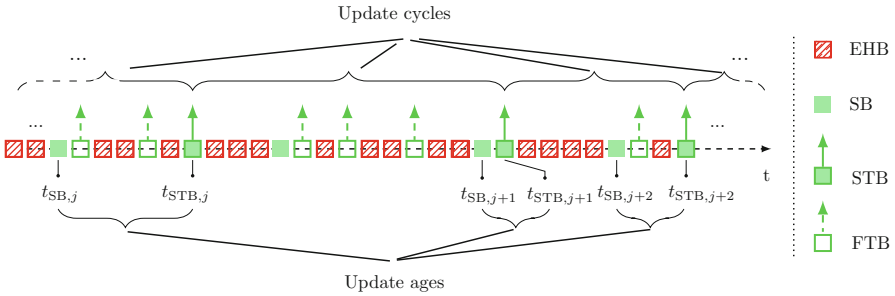

Fig. 8.8 Illustration of the sensing and transmission protocol, and the update cycle and update age

blocks, a new SB occurs, after which, however, a STB never occurs within 6 time blocks. Therefore, the sensed packet has to be dropped. In other words, the sensed information in the second SB is not able to be received by the sink.

The time indices shown in Fig. 8.8 will be defined in the following section.

8.5.3 Delay Related Metrics

As discussed in Sect. 8.4.2, to completely capture the timeliness of the status monitoring WSN, we need both the update cycle and the update age metrics. Recall that update age measures the time taken from when information is obtained by the sensor to when the sensed information is successfully transmitted to the sink, i.e., how timely the updated information at the sink is, and update cycle measures the time duration between two consecutive successful transmissions, i.e., how frequently the information at the sink is updated. Thus, both the metrics are important for measuring the timeliness of the status monitoring WSN.

As shown in Fig. 8.8, for the ease of describing the two metrics, $t_{\mathrm{STB},j}$ is used to denote the block index for the jth STB during the entire sensing and transmission operation. Since each STB corresponds to a SB that generates the status information contained in the STB, $t_{\mathrm{SB},j}$ is used to denote the block index for the SB in which the sensed information is transmitted in the jth STB.

The two delay related metrics, expressed in terms of the number of time blocks, are formally defined in the following.

Definition 1 (Update Age). For the jth STB, the update age is given by the number of time blocks from $t_{\mathrm{SB},j}$ to $t_{\mathrm{STB},j}$ (shown in Fig. 8.8). The jth update age is

$$T_{\mathrm{UA},j} = t_{\mathrm{STB},j} - t_{\mathrm{SB},j},\ j = 1, 2, 3, \ldots. \tag{8.7}$$

Remark 1. Conditioned on a successful status-information-containing packet reception at the sink, the update age measures the time elapsed from the generation of the packet at the sensor to the successful reception of the packet at the sink. A larger update age implies that a more outdated status is received by the sink. However, the update age does not capture the delay that caused by dropped data packets, and hence is not able to reflect the update frequency at the sink.

Definition 2 (Update Cycle). For the jth STB, the update cycle is given by the number of time blocks from $t_{\mathrm{STB},j-1}$ to $t_{\mathrm{STB},j}$ (shown in Fig. 8.8). The jth update cycle is

$$T_{\mathrm{UC},j} = t_{\mathrm{STB},j+1} - t_{\mathrm{STB},j},\ j = 1, 2, 3, \ldots. \tag{8.8}$$

Remark 2. The update cycle measures the time elapsed from one successful status update at the sink to the next, which takes into account the delay due to dropped data packets. However, the update cycle is not able to measure the update freshness at the sink, i.e., the time duration from the generation of a packet to its successful reception at the sink.

Therefore, update age and update cycle complement each other, and they jointly capture the update freshness and frequency. Using both the metrics provides comprehensive measure of the performance of a status monitoring WSN.

8.5.3.1 Modeling Update Age and Update Cycle as i.i.d. Random Variables

To study the steady-state behavior of the update age and the update cycle during the sensing and transmission process, we need the following lemma first.

Lemma 1. For an exponential energy arrival process, the steady-state distribution of the energy level after each TB has pdf

$$g(\varepsilon) = \frac{1}{\rho} e^{-\frac{\varepsilon}{\rho}}, \tag{8.9}$$

where ρ is the average harvested energy.

Proof. This proof is identical to [59, Lemma 1]. We repeat some of the details here for sake of completeness.

Because the harvested energy in each EHB is an exponentially distributed random variable with parameter ρ, as we have mentioned in Sect. 8.5.1, the energy accumulation process by consecutive EHBs can be treated as a Poisson process [60]. Using the memorylessness property of the Poisson process [60, p. 134], conditioned on that the available energy is higher than any given threshold value, the amount of energy exceeding that threshold has the same distribution with the harvested energy in each time block, i.e., Eq. (8.9). This completes the proof of Lemma 1.

From the definitions of the update age and the update cycle, $T_{\mathrm{UA},j}$ and $T_{\mathrm{UC},j}$ only depend on (1) the available energy after the first TB following a SB, and (2) the random EH process after the TB. Since the steady-state distribution after each TB is the same (i.e., Lemma 1) and the EH process is a steady-state process (i.e., the i.i.d. exponential energy arrival process), both $T_{\mathrm{UA},j}$ and $T_{\mathrm{UC},j}$ have steady-state distributions. For convenience, we remove subscript j for T_{UA} and T_{UC} in (8.7) and (8.8), respectively.

8.5.4 Delay Analysis

We present the analytical results of the update age and the update cycle in this section.

8.5.4.1 Update Age and Update Cycle

Theorem 1. *For an exponential energy arrival process, average update age is given by*

$$\bar{T}_{\mathrm{UA}} = \frac{(1-P_{\mathrm{out}})}{P_{\mathrm{suc}}}\left(1+\sum_{l=2}^{W} l \sum_{n=2}^{l} (P_{\mathrm{out}})^{n-1}\,\mathrm{Pois}\left(l-n,(n-1)\mathscr{E}_{\mathrm{TB}}/\rho\right)\right) \tag{8.10}$$

where

$$P_{\mathrm{suc}} = 1-P_{\mathrm{out}}+(1-P_{\mathrm{out}})\sum_{l=2}^{W}\sum_{n=2}^{l}(P_{\mathrm{out}})^{n-1}\,\mathrm{Pois}\left(l-n,(n-1)\mathscr{E}_{\mathrm{TB}}/\rho\right). \tag{8.11}$$

From Theorem 1, the average update age is independent with the energy cost of sensing.

Theorem 2. *For an exponential energy arrival process, average update cycle is given by*

$$\bar{T}_{\mathrm{UC}} = \frac{1-P_{\mathrm{suc}}}{P_{\mathrm{suc}}}\left(\frac{\mathscr{E}_{\mathrm{SB}}}{\rho}+\bar{V}+W+1\right)+\frac{\mathscr{E}_{\mathrm{SB}}+\mathscr{E}_{\mathrm{TB}}}{\rho}+\bar{T}_{\mathrm{UA}}+1, \tag{8.12}$$

where $\bar{T}_{\mathrm{UA}}$ *and* P_{suc} *are given in* (8.10) *and* (8.11)*, and*

$$\begin{aligned}\bar{V} = {} & \frac{P_{\mathrm{out}}}{1-P_{\mathrm{suc}}}\left(\frac{\mathscr{E}_{\mathrm{TB}}}{\rho}-\sum_{i=0}^{W-2} i\mathrm{Pois}\left(i,\frac{\mathscr{E}_{\mathrm{TB}}}{\rho}\right)-(W-1)\left(1-\sum_{i=0}^{W-2}\mathrm{Pois}\left(i,\frac{\mathscr{E}_{\mathrm{TB}}}{\rho}\right)\right)\right)\\ & +\frac{1}{1-P_{\mathrm{suc}}}\times\sum_{l=2}^{W}\sum_{n=2}^{l}(P_{\mathrm{out}})^{n}\,\mathrm{Pois}\left(l-n,(n-1)\frac{\mathscr{E}_{\mathrm{TB}}}{\rho}\right)\Phi_l,\end{aligned} \tag{8.13}$$

where

$$\Phi_l \triangleq \left(\frac{\mathscr{E}_{\mathrm{TB}}}{\rho}-\sum_{i=0}^{W-l-1} i\mathrm{Pois}\left(i,\frac{\mathscr{E}_{\mathrm{TB}}}{\rho}\right)-(W-l)\left(1-\sum_{i=0}^{W-l-1}\mathrm{Pois}\left(i,\frac{\mathscr{E}_{\mathrm{TB}}}{\rho}\right)\right)\right). \tag{8.14}$$

Proof. See Appendix F of [48].

From Theorem 2, the average update cycle depends on both the energy cost of sensing and transmission.

8.5.4.2 Asymptotic Update Age and Update Cycle

We also present the asymptotic update age and update cycle when the retransmission window $W-1$ is sufficiently large.

Corollary 1. *For an exponential energy arrival process, $\bar{T}_{\mathrm{UA}}$ increases with W, and as W gets large, the asymptotic $\bar{T}_{\mathrm{UA}}$ is given by*

$$\lim_{W\to\infty} \bar{T}_{\mathrm{UA}} = 1 + \frac{P_{\mathrm{out}}}{1-P_{\mathrm{out}}}\left(\frac{\mathscr{E}_{\mathrm{TB}}}{\rho}+1\right). \tag{8.15}$$

Proof. See Appendix G of [48].

Corollary 2. *For an exponential energy arrival process, $\bar{T}_{\mathrm{UC}}$ decreases with W, and as W grows large, the asymptotic $\bar{T}_{\mathrm{UC}}$ is given by*

$$\lim_{W\to\infty} \bar{T}_{\mathrm{UC}} = 2 + \frac{\mathscr{E}_{\mathrm{SB}}+\mathscr{E}_{\mathrm{TB}}}{\rho} + \frac{P_{\mathrm{out}}}{1-P_{\mathrm{out}}}\left(\frac{\mathscr{E}_{\mathrm{TB}}}{\rho}+1\right). \tag{8.16}$$

Proof. See Appendix G of [48].

8.5.4.3 Numerical Results

In this section, we present numerical results for the update age and update cycle. We set the distance between the sensor and the sink as $d = 90\,\mathrm{m}$. This is because the typical outdoor range for a wireless sensor is from 75 to 100 m [61]. Also we set the path loss exponent for the sensor-sink transmission link as $\lambda = 3$ [31]. The noise power at the sink is $\sigma^2 = -100\,\mathrm{dBm}$ [40]. The duration of a time block is $T = 5\,\mathrm{ms}$[14]. The average harvested power is 10 mW [62], i.e., average harvested energy per time block, $\rho = 50\,\mu\mathrm{J}$. The RF-DC sensitivity level is $-20\,\mathrm{dBm}$ [28]. Unless otherwise stated, (1) we set the power consumption in each TB, $\mathscr{P}_{\mathrm{TB}} = 40\,\mathrm{mW}$, i.e., $\mathscr{E}_{\mathrm{TB}} = 200\,\mu\mathrm{J}$. Note that this includes RF circuit consumption (main consumption) and the actual RF transmit power $\mathscr{P}_{\mathrm{tx}} = -5\,\mathrm{dBm}$[1] and (2) we set the power consumption in each SB as $\mathscr{P}_{\mathrm{SB}} = 45\,\mathrm{mW}$[8], i.e., $\mathscr{E}_{\mathrm{SB}} = 225\,\mu\mathrm{J}$. In the following calculations, power and SNR related quantities use a linear scale.

Assuming the SNR threshold $\gamma = 40\,\mathrm{dB}$ [57], we apply (8.6) to Theorems 1–2 and Corollaries 1–2, we compute the expressions of average and the asymptotic values of T_{UA} and T_{UC}.

Pmfs of Update Age and Update Cycle Figure 8.9 plots the pmfs of update cycle, T_{UC}, and update age, T_{UA}, for the exponential energy arrival process, respectively. The results are plotted using Monte Carlo simulation method with 10^9 points. We

[1]The values we chose for $\mathscr{P}_{\mathrm{TB}}$ and $\mathscr{P}_{\mathrm{tx}}$ are typical for commercial sensor platforms, such as MICAz [61].

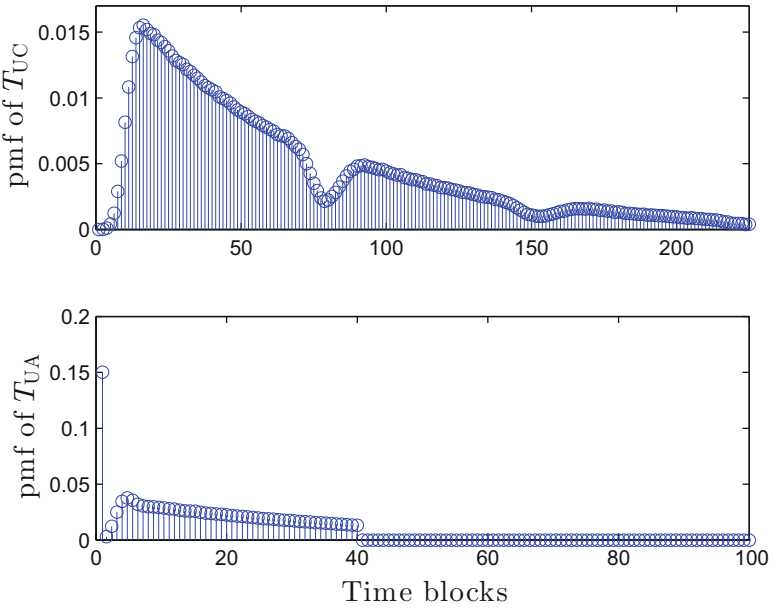

Fig. 8.9 Pmfs for T_{UC} and T_{UA}

set $W = 40$, i.e., the time window for retransmissions is $W - 1 = 39$ time blocks. We see that the pmfs in general cannot be modeled by commonly used pmfs, such as Poison distribution.

In the following figures, i.e., Figs. 8.7 and 8.8, we only present the numerical results for the average update age and the average update cycle, which have been presented in Corollaries 1–2.

Average Update Age and Average Update Cycle Figure 8.10 shows the average update age, $\bar{T}_{\mathrm{UA}}$, and the average update cycle, $\bar{T}_{\mathrm{UC}}$, for different W, i.e., different retransmission window, $W - 1$. The results are generated using Theorems 1 and 2 and Corollaries 1 and 2, respectively. We can see that as the time window for retransmissions increases, the average update age increases monotonically and approaches its asymptotic value given by Corollary 1, while the average update cycle decreases monotonically and approaches its analytical lower bound given by Corollary 2. Also we see that with a larger retransmission window $W-1$, the updated status is in general less fresh, but the update frequency is higher.

Effect of Energy Cost of Sensing on Average Update Cycle We illustrate the effect of energy cost of sensing on average update cycle. Figure 8.11 shows the average update age, $\bar{T}_{\mathrm{UA}}$, and the average update cycle, $\bar{T}_{\mathrm{UC}}$, versus W, with different energy cost of sensing, $\mathscr{P}_{\mathrm{SB}}T$. The results are generated using Theorems 1 and 2. The figure shows that the average update age increases with W, which is consistent with Fig. 8.10, but it does not change with the energy cost of sensing, i.e., *the update*

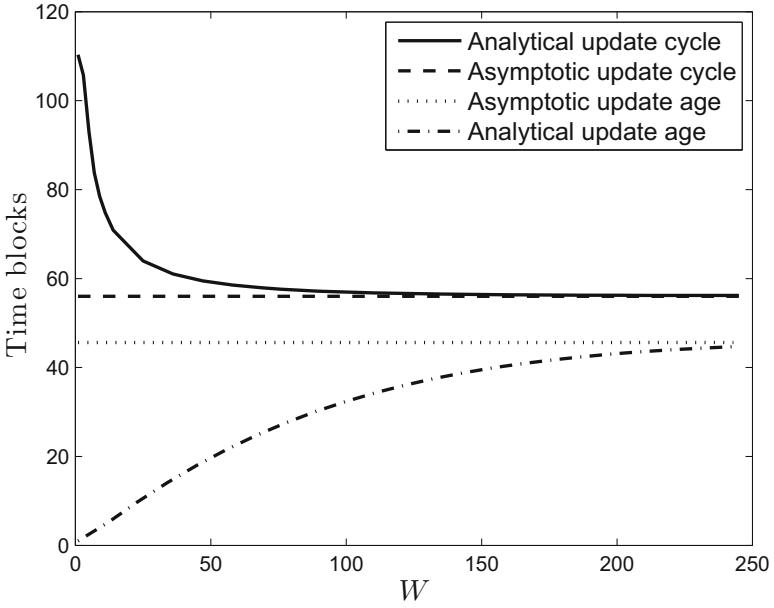

Fig. 8.10 $\bar{T}_{\mathrm{UA}}$ and $\bar{T}_{\mathrm{UC}}$, versus W

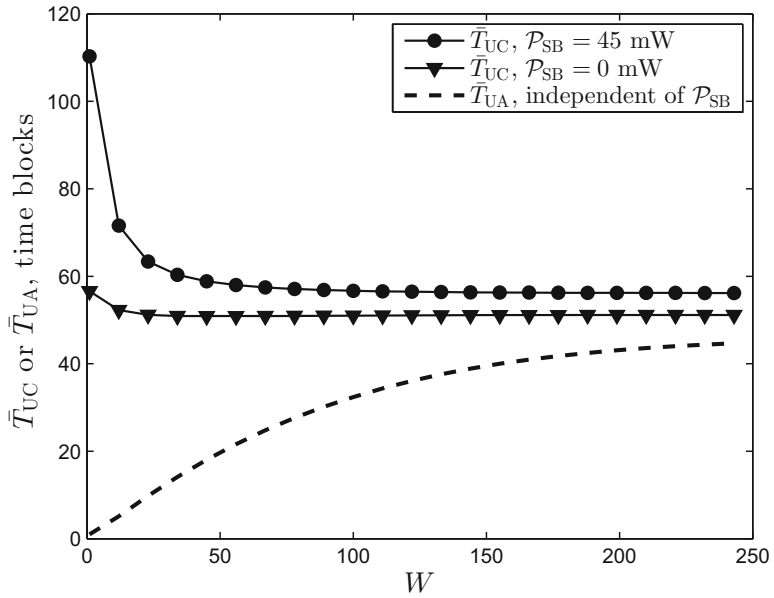

Fig. 8.11 $\bar{T}_{\mathrm{UC}}$ and $\bar{T}_{\mathrm{UA}}$ versus W for different sensing power, $\mathscr{P}_{\mathrm{SB}}$

age does not rely on the energy cost of sensing. This is because the update age is the delay after a SB, and is independent with the energy cost of sensing. We can see that for a fixed value of W, e.g., $W = 50$, the average update cycle increases as the sensing power consumption increases from 0 to 45 mW, i.e., *the higher the energy cost of sensing the larger update cycle.* This is because during an update cycle several SB occurs, and the higher energy cost of sensing the more EHBs within the update cycle. We can see that $\bar{T}_{\mathrm{UC}}$ is almost constant around the value of 52 and does not vary much with W, i.e., the effect retransmission window on the average update cycle is limited when the energy cost of sensing is ignored.

Summary

In this chapter, we have discussed the basic architecture of EH-based WSNs and wireless power transfer-based WSNs. We have highlighted the advantage and suitability of wireless power transfer-based WSNs, and discussed the associated design challenges. We have presented a novel solution to one of the challenges, related to the timeliness of the status monitoring WSNs, i.e., update cycle and update age. Moreover, we have presented a framework of analysis for both the update cycle and the update age, which takes into account both the energy cost of sensing and transmission.

References

1. K. Sohraby, D. Minoli, T. Znati, *Wireless Sensor Networks: Technology, Protocols, and Applications* (Wiley, New York, 2007)
2. M. Connectivity, The monitored World - a local perspective (2015). [Online]. Available: https://blog.m2mconnectivity.com.au/2015/09/07/the-monitored-world-a-local-perspective/
3. H. Yetgin, K.T.K. Cheung, M. El-Hajjar, L. Hanzo, A survey of network lifetime maximization techniques. IEEE Commun. Surv. Tutorials. (2017). Accepted
4. S. Sudevalayam, P. Kulkarni, Energy harvesting sensor nodes: survey and implications. IEEE Commun. Surv. Tutorials **13**(3), 443–461, Third Quarter (2011)
5. V. Gungor, G. Hancke, Industrial wireless sensor networks: challenges, design principles, and technical approaches. IEEE Trans. Ind. Electron. **56**(10), 4258–4265 (2009)
6. D. Niyato, E. Hossain, A. Fallahi, Sleep and wakeup strategies in solar-powered wireless sensor/mesh networks: performance analysis and optimization. IEEE Trans. Mob. Comput. **6**(2), 221–236 (2007)
7. J. Lei, R. Yates, L. Greenstein, A generic model for optimizing single-hop transmission policy of replenishable sensors. IEEE Trans. Wirel. Commun. **8**(2), 547–551 (2009)
8. V. Raghunathan, S. Ganeriwal, M. Srivastava, Emerging techniques for long lived wireless sensor networks. IEEE Commun. Mag. **44**(4), 108–114 (2006)
9. W. Liu, K. Huang, X. Zhou, S. Durrani, Backscatter communications for internet-of-things: theory and applications. ArXiv e-prints (2017). [Online]. Available: https://arxiv.org/abs/1701.07588

10. C. Boyer, S. Roy, Backscatter communication and RFID: coding, energy, and MIMO analysis. IEEE Trans. Commun. **62**(3), 770–785 (2014)
11. W. Liu, K. Huang, X. Zhou, S. Durrani, Full-duplex backscatter interference networks based on time-hopping spreading spectrum. IEEE Trans. Wirel. Commun. (2017, to appear)
12. S. Mao, M.H. Cheung, V. Wong, Joint energy allocation for sensing and transmission in rechargeable wireless sensor networks. IEEE Trans. Veh. Technol. **63**(6), 2862–2875 (2014)
13. H. Mahdavi-Doost, R. Yates, Energy harvesting receivers: finite battery capacity, in *Proceedings of IEEE ISIT*, July (2013), pp. 1799–1803
14. Z.A. Eu, H.-P. Tan, W.K. Seah, Design and performance analysis of MAC schemes for wireless sensor networks powered by ambient energy harvesting. Ad Hoc Netw. **9**(3), 300–323 (2011)
15. C. Huang, R. Zhang, S. Cui, Throughput maximization for the Gaussian relay channel with energy harvesting constraints. IEEE J. Sel. Areas Commun. **31**(8), 1469–1479 (2013)
16. C.K. Ho, R. Zhang, Optimal energy allocation for wireless communications with energy harvesting constraints. IEEE Trans. Signal Process. **60**(9), 4808–4818 (2012)
17. A. Seyedi, B. Sikdar, Energy efficient transmission strategies for body sensor networks with energy harvesting. IEEE Trans. Commun. **58**(7), 2116–2126 (2010)
18. S. Zhang, A. Seyedi, B. Sikdar, An analytical approach to the design of energy harvesting wireless sensor nodes. IEEE Trans. Wirel. Commun. **12**(8), 4010–4024 (2013)
19. S. Luo, R. Zhang, T.J. Lim, Optimal save-then-transmit protocol for energy harvesting wireless transmitters. IEEE Trans. Wirel. Commun. **12**(3), 1196–1207 (2013)
20. R. Morsi, D. Michalopoulos, R. Schober, On-off transmission policy for wireless powered communication with energy storage, in *Proceedings of Asilomar*, November (2014), pp. 1676–1682
21. Y. Dong, F. Farnia, A. Ozgur, Near optimal energy control and approximate capacity of energy harvesting communication. IEEE J. Sel. Areas Commun. **33**(3), 540–557 (2015)
22. N. Michelusi, L. Badia, M. Zorzi, Optimal transmission policies for energy harvesting devices with limited state-of-charge knowledge. IEEE Trans. Commun. **62**(11), 3969–3982 (2014)
23. O. Ozel, K. Tutuncuoglu, J. Yang, S. Ulukus, A. Yener, Transmission with energy harvesting nodes in fading wireless channels: optimal policies. IEEE J. Sel. Areas Commun. **29**(8), 1732–1743 (2011)
24. J. Yang, S. Ulukus, Transmission completion time minimization in an energy harvesting system, in *Proceedings of CISS*, March (2010), pp. 1–6
25. J. Yang, S. Ulukus, Delay-minimal transmission for energy constrained wireless communications, in *Proceedings of IEEE ICC*, May (2008), pp. 3531–3535
26. Y. Mao, G. Yu, Z. Zhang, On the optimal transmission policy in hybrid energy supply wireless communication systems. IEEE Trans. Wirel. Commun. **13**(11), 6422–6430 (2014)
27. N. Michelusi, M. Zorzi, Optimal random multiaccess in energy harvesting wireless sensor networks, in *Proceedings of IEEE ICC*, June (2013), pp. 463–468
28. X. Lu, P. Wang, D. Niyato, D.I. Kim, Z. Han, Wireless networks with RF energy harvesting: a contemporary survey. IEEE Commun. Surv. Tutorials **17**(2), 757–789, Second Quarter (2015)
29. B. Clerckx, E. Bayguzina, Waveform design for wireless power transfer. IEEE Trans. Signal Process. **64**(23), 6313–6328 (2016)
30. E. Boshkovska, D.W.K. Ng, N. Zlatanov, R. Schober, Practical non-linear energy harvesting model and resource allocation for SWIPT systems. IEEE Commun. Lett. **19**(12), 2082–2085 (2015)
31. T. Wu, H.-C. Yang, On the performance of overlaid wireless sensor transmission with RF energy harvesting. IEEE J. Sel. Areas Commun. **33**(8), 1693–1705 (2015)
32. W. Liu, X. Zhou, S. Durrani, P. Popovski, SWIPT with practical modulation and RF energy harvesting sensitivity, in *Proceedings of ICC*, May (2016), pp. 1–7
33. R. Zhang, C.K. Ho, MIMO broadcasting for simultaneous wireless information and power transfer. IEEE Trans. Wirel. Commun. **12**(5), 1989–2001 (2013)
34. X. Zhou, R. Zhang, C.K. Ho, Wireless information and power transfer: architecture design and rate-energy tradeoff. IEEE Trans. Commun. **61**(11), 4754–4767 (2013)
35. K. Huang, V.K.N. Lau, Enabling wireless power transfer in cellular networks: architecture, modeling and deployment. IEEE Trans. Wirel. Commun. **13**(2), 902–912 (2014)

36. J. Xu, R. Zhang, Energy beamforming with one-bit feedback. IEEE Trans. Signal Process. **62**(20), 5370–5381 (2014)
37. S. Lee, R. Zhang, Distributed energy beamforming with one-bit feedback, in *Proceedings of IEEE WCNC*, April (2016), pp. 1–6
38. Z. Wang, L. Duan, R. Zhang, Adaptively directional wireless power transfer for large-scale sensor networks. IEEE J. Sel. Areas Commun. **34**(5), 1785–1800 (2016)
39. S. Bi, R. Zhang, Placement optimization of energy and information access points in wireless powered communication networks. IEEE Trans. Wirel. Commun. **15**(3), 2351–2364 (2016)
40. A.A. Nasir, X. Zhou, S. Durrani, R.A. Kennedy, Wireless-powered relays in cooperative communications: time-switching relaying protocols and throughput analysis. IEEE Trans. Commun. **63**(5), 1607–1622 (2015)
41. Y. Zeng, H. Chen, R. Zhang, Bidirectional wireless information and power transfer with a helping relay. IEEE Commun. Lett. **20**(5), 862–865 (2016)
42. S. Luo, J. Xu, T.J. Lim, R. Zhang, Capacity region of MISO broadcast channel for simultaneous wireless information and power transfer. IEEE Trans. Commun. **63**(10), 3856–3868 (2015)
43. X. Zhou, C.K. Ho, R. Zhang, Wireless information and power transfer in multiuser OFDM systems. IEEE Trans. Wirel. Commun. **13**(4), 2282–2294 (2014)
44. K. Huang, E. Larsson, Simultaneous information and power transfer for broadband wireless systems. IEEE Trans. Signal Process. **61**(23), 5972–5986 (2013)
45. H. Ju, R. Zhang, Throughput maximization in wireless powered communication networks. IEEE Trans. Wirel. Commun. **13**(1), 418–428 (2014)
46. I. Krikidis, Simultaneous information and energy transfer in large-scale networks with/without relaying. IEEE Trans. Commun. **62**(3), 900–912 (2014)
47. W. Liu, X. Zhou, S. Durrani, P. Popovski, Secure communication with a wireless-powered friendly jammer. IEEE Trans. Wirel. Commun. **15**(1), 401–415 (2016)
48. W. Liu, X. Zhou, S. Durrani, H. Mehrpouyan, S.D. Blostein, Energy harvesting wireless sensor networks: delay analysis considering energy costs of sensing and transmission. IEEE Trans. Wirel. Commun. **15**(7), 4635–4650 (2016)
49. A. Nasir, X. Zhou, S. Durrani, R. Kennedy, Wireless-powered relays in cooperative communications: time-switching relaying protocols and throughput analysis. IEEE Trans. Commun. **63**(5), 1607–1622 (2015)
50. Y. Zeng, R. Zhang, Optimized training design for wireless energy transfer. IEEE Trans. Commun. **63**(2), 536–550 (2015)
51. Y. Zeng, R. Zhang, Optimized training for net energy maximization in multi-antenna wireless energy transfer over frequency-selective channel. IEEE Trans. Commun. **63**(6), 2360–2373 (2015)
52. J. Xu, R. Zhang, A general design framework for MIMO wireless energy transfer with limited feedback. IEEE Trans. Signal Process. **64**(10), 2475–2488 (2016)
53. M. Costa, M. Codreanu, A. Ephremides, Age of information with packet management, in *Proceedings of ISIT*, June (2014), pp. 1583–1587
54. S. Kaul, R. Yates, M. Gruteser, Real-time status: How often should one update? in *Proceedings of IEEE INFOCOM*, March (2012), pp. 2731–2735
55. Y. Sun, E. Uysal-Biyikoglu, R. Yates, C.E. Koksal, N.B. Shroff, Update or wait: how to keep your data fresh, in *Proceedings of IEEE INFOCOM*, April (2016), pp. 1–9
56. P. Lee, Z.A. Eu, M. Han, H. Tan, Empirical modeling of a solar-powered energy harvesting wireless sensor node for time-slotted operation, in *Proceedings of IEEE WCNC*, March (2011), pp. 179–184
57. Z. Ding, S. Perlaza, I. Esnaola, H.V. Poor, Power allocation strategies in energy harvesting wireless cooperative networks. IEEE Trans. Wirel. Commun. **13**(2), 846–860 (2014)
58. A.J. Goldsmith, *Wireless Communications* (Cambridge University Press, New York, 2005)

59. W. Liu, X. Zhou, S. Durrani, H. Mehrpouyan, S.D. Blostein, Performance of wireless-powered sensor transmission considering energy cost of sensing, in *Proceedings of IEEE GLOBECOM*, December (2015), pp. 1–7
60. R. Durrett, *Probability: Theory and Examples* (Cambridge University Press, Cambridge, 2010)
61. MICAz, Crossbow Technology (2006). [Online]. Available: http://www.openautomation.net/uploadsproductos/micaz-datasheet.pdf
62. F. Zhang, V. Lau, Closed-form delay-optimal power control for energy harvesting wireless system with finite energy storage. IEEE Trans. Signal Process. **62**(21), 5706–5715 (2014)